Journal of Molecular Catalysis A: Chemical 429 (2017) 1–9

Contents lists available at ScienceDirect

Journal of Molecular Catalysis A: Chemical

journal homepage: www.elsevier.com/locate/molcata

Editor's choice paper

Hydrogen production on alumina-supported platinum catalysts

André Rosa Martins[a,b], Luciene Santos Carvalho[a,b], Patrício Reyes[c], Javier Mario Grau[d], Maria do Carmo Rangel[a,*]

[a] GECCAT Grupo de Estudos em Cinética e Catálise, Instituto de Química, Universidade Federal da Bahia, Rua Barão de Geremoabo, 147, Campus Universitário de Ondina, Federação, 40170-290 Salvador, Bahia, Brazil
[b] GPMAC Grupo de Pesquisa em Materiais e Catálise, Instituto Federal de Educação, Ciência e Tecnologia da Bahia, Campus Camaçari, Loteamento Espaço Alpha, BA 522, Limoeiro, 42802-590 Camaçari, Bahia, Brazil
[c] Facultad de Ciencias Químicas, Universidad de Concepción, Casilla 3-C, Concepción, Chile
[d] Instituto de Investigaciones en Catálisis y Petroquímica "Ing. José Miguel Parera"—INCAPE, Facultad de Ingeniería Química—FIQ, Universidad Nacional del Litoral—UNL, Colectora Ruta Nacional No 168, Km 0, Paraje El Pozo, 3000, Santa Fe, Argentina

ARTICLE INFO

Article history:
Received 4 October 2016
Received in revised form
19 November 2016
Accepted 30 November 2016
Available online 1 December 2016

Keywords:
Hydrogen
Alumina
Platinum
Steam reforming
Al-Mg spinel

ABSTRACT

Hydrogen production is commercially performed by methane steam reforming over alumina-supported nickel catalysts, which deactivate by coke requiring improved catalysts. Aiming to find alternative catalysts for the reaction, the properties of Pt/Al_2O_3-MgO catalysts were studied in this work. It was found that small amounts of magnesium (Al/Mg (molar) = 5) enter into alumina lattice and produce magnesium aluminate on the surface. For higher amounts (Al/Mg = 2) only magnesium aluminate is produced. For even higher contents (Al/Mg = 0.2) aluminum enters into magnesia lattice, producing magnesia and magnesium aluminate on the surface. The specific surface area, acidity and platinum dispersion changed with magnesium amount, the aluminum-richest catalyst (Al/Mg = 5) showing the highest values. Consequently, the activity and selectivity of the catalysts change in methane steam reforming and in water gas shift reaction, different values of products yield and H_2/CO being obtained. The sample with Al/Mg = 5 is the most promising catalyst to produce hydrogen.

1. Introduction

In recent years, the interest for producing pure hydrogen has been increasing fast, as a consequence of the ultimate goal of developing a hydrogen economy, which is expected to play a crucial role in the future energy supply. Although molecular hydrogen is very rare in the earth atmosphere, it is considered an inexhaustible fuel, because it can be obtained from a large variety of abundant searches in the earth, such as biomass, water, natural gas, biogas and oil, among others [1,2]. In addition, hydrogen is an efficient, cost attractive and a clean burning fuel, which can be stored as a liquid or gas. Despite the current pipeline infrastructure is not suitable for its storage and distribution, hydrogen is considered as a long term substitute for natural gas [1,3]. Nowadays, hydrogen is widely used as feedstock in the chemical, food and refining industries, besides in the steel and electronics industries [3,4].

Hydrogen can be obtained from both fossil sources (such as oil-derived methane and natural gas) or renewable sources, like biogas or biomass [1]. However, due to the great reserves worldwide, natural gas is still the most important feed for hydrogen production. In addition, the shale gas development in last decade, especially in North America, has increased assessments of resources producible at low cost. Therefore, it is expected that the use of natural gas continues to expand in the future [5].

Methane steam reforming is currently the main commercial route for producing hydrogen. During the process, a mixture of hydrogen, carbon monoxide and carbon dioxide is produced from natural gas or other feedstocks, in the presence of steam. The main reaction, shown in Eq. (1), is highly endothermic and thus high temperatures favor the reaction. The water gas shift reaction (WGSR), Eq. (2), can also occur in the operation conditions [6]. For both cases, a high steam to carbon molar ratio shifts the thermodynamic equilibrium favoring hydrogen production and then a rich effluent in hydrogen is produced.

$$CH_{4(g)} + H_2O_{(g)} \rightleftarrows CO_{(g)} + 3H_{2(g)} \Delta H = +206\, kJ\, mol^{-1} \quad (1)$$

$$CO_{(g)} + H_2O_{(g)} \rightleftarrows CO_{2(g)} + H_{2(g)} \Delta H = -41\, kJ\, mol^{-1} \quad (2)$$

The classical catalysts used in steam reforming are nickel based solids which show high activity and low cost. The metal is often

* Corresponding author.
E-mail addresses: mcarmov@ufba.br, mcarmog@gmail.com (M.d.C. Rangel).

http://dx.doi.org/10.1016/j.molcata.2016.11.040
1381-1169/

dispersed on supports able to provide the thermal and mechanical resistance required by the operation conditions, such as high temperatures. Alumina is by far the most used support since it is able to fit these requirements [6].

The major problem of the steam reforming is the fast catalyst deactivation by coke deposition, which blocks the pores preventing the access of the reactants to the active sites. This process occurs through several reactions that can take place on the catalyst surface, such as the dissociative adsorption of methane (Eq. (3)), the Boudouard reaction (Eq. (4)), the reduction of carbon monoxide (Eq. (5)) and the decomposition of hydrocarbons (Eq. (6)) [7]. In order to decrease coke production, the process is often carried out in the presence of steam. Therefore, the industrial reformers usually work under steam to carbon molar ratios in the range of 2–5 [6]. However, the steam and the severe operating conditions favor other deactivation processes such as the sintering of the metal and of the support, which decreases the active surface area. As a consequence, the control of thermal stability has become as important as controlling the activity and selectivity [7].

$$CH_4 \rightleftarrows C + 2H_2 \quad (3)$$

$$2CO \rightleftarrows C + CO_2 \quad (4)$$

$$CO + H_2 \rightleftarrows C + H_2O \quad (5)$$

$$C_nH_{2n+2} \rightleftarrows nC + (n+1)H_2O \quad (6)$$

Aiming to achieve the required properties for the steam reforming catalysts, several works have been devoted to improving the performance of nickel-based catalysts [8–10] as well as to find other metals that can replace nickel [11,12]. Noble metals, in special, are attractive options to reforming catalysts due to their activities for catalyzing coke gasification. Previous works [12,13] have shown that less coke was deposited on noble metals based catalysts such as platinum, rhodium, ruthenium and palladium deposited on several supports. Platinum has also been successfully used as active phase in dry reforming of methane [14,15], partial oxidation of methane [16,17], combined partial oxidation and dry reforming, oxidative steam reforming of methane [18] and in reforming of ethanol [19], methanol [20], glycerol [21] and biomass [22]. However, some coke deposition was still found, depending on the support.

On the other hand, since basic solids catalyze the gasification of carbon [7], they can prevent coke deposition on the catalyst surface and then the support for reforming catalysts should be chosen considering this property. Among the basic solids, magnesium oxide emerges as an attractive option, since it has strong basic sites due to O^{2-} ions and easiness in receiving protons [9,10,23]. If the magnesium oxide basicity is combined with the high thermal stability and the specific surface area of alumina, a promising combination results for reforming catalysts. Indeed, magnesium aluminate spinels show low acidity and high stability in the high temperatures of the process and then have been considered for the reaction [12,24].

In a previous work [12], we have found that supports based on aluminum and magnesium oxides were suitable for ruthenium-based catalysts for steam reforming. In the present work, we investigated the properties of platinum-based catalysts supported on aluminum and magnesium oxide. It is expected to find catalysts with high selectivity to hydrogen production and with resistance against coke deactivation, by combining the properties of magnesium oxide and platinum.

2. Material and methods

2.1. Catalysts preparation

The preparation of the supports with aluminum to magnesium molar ratio of 5 (AM5 sample), 2 (AM2) and 0.2 (AM02) and alumina (A) and magnesia (M) was described elsewhere [12]. The catalysts were obtained by incipient wet impregnation technique using 3 mL of hexachloroplatinic acid solution (H_2PtCl_6) for gram of the support, in order to obtain platinum (1% w/w) catalysts. After impregnation, the solvent was evaporated and the solids were dried at 120 °C, for 24 h and calcined at 600 °C under air flow, during 8 h.

2.2. Catalysts characterization

The fresh catalysts were characterized by X-ray diffraction, specific surface area measurements, temperature programmed reduction, acidity measurements by temperature programmed desorption of ammonia, Fourier transform infrared spectroscopy of adsorbed carbon monoxide, metal dispersion measurements, X-ray photoelectron spectroscopy and by the model reaction of cyclohexane dehydrogenation. After steam methane reforming, the coke deposited on the spent catalysts was determined by chemical analysis.

The X-ray diffractograms (XRD) were obtained using a Shimadzu model XRD600 equipment and a nickel filter. The sample was exposed to CuKα radiation generated at 30 kV and 20 mA, from 2θ of 10–80°. Other experiments, using a heating chamber were also performed, heating the solids in situ under air flow (60 mL min^{-1}), at 10 °C min^{-1} and collecting the diffractograms at 450, 550, 650, 750 and 850 °C. The specific surface area (Sg) measurements were carried out by physical nitrogen adsorption (BET method). During the experiments, a Micromeritics model AZAP 2020 apparatus was used on 0.3 g of sample, previously heated under vacuum at 200 °C, for 1 h.

The experiments of temperature programmed reduction (TPR) of the catalysts were performed in a Micromeritics model TPD/TPR 2900 equipment, equipped with thermal conductivity detector (TCD). Samples (0.25–0.3 g) were reduced in the range of 30–600 °C, at 10 °C min^{-1}, under a 5% H_2/N_2 mixture flow. The hydrogen consumption in the experiments was calculated from the area under the peaks, using the calibration curve obtained with a cooper oxide (CuO) standard. The acidity of the samples was determined by ammonia temperature programmed desorption (TPD-NH_3) using the same equipment. The sample (0.05 g) was heated up to 300 °C, under helium flow and cooled to room temperature. It was then heated up to 110 °C under the same gas flow and saturated with ammonia, by the injection through a calibrated loop. The system was heated up to 775 °C, under helium flow, for obtaining the ammonia TPD profile. The acidity was calculated from the areas of the adsorption peaks for ammonia, taking the last peak for calibration.

The Fourier transform infrared spectroscopy (FTIR) experiments of adsorbed carbon monoxide on the metallic surface were performed in a Perkin-Elmer model Spectrum One equipment. The sample (0.08 g) was prepared as a self-supporting wafer under a pressure of 8 t, for 5 min. Before analysis, the sample was reduced during 2 h, at 600 °C, under hydrogen flow (60 mL min^{-1}). After reduction, the hydrogen excess was removed by vacuum (10^{-5} Torr), for 30 min. At this stage, a pulse of carbon monoxide of 50 mbar was injected for 5 min. The spectra were registered with a 4 cm^{-1} resolution before and after carbon monoxide chemisorption and the final spectrum was obtained by subtracting those spectra.

The metal dispersion of the catalysts was determined by carbon monoxide chemisorption, at 25 °C and atmospheric pressure. In the experiments, the sample (0.1 g) was previously reduced in

hydrogen flow at 600 °C, for 1 h. After cooling in nitrogen flow up to room temperature, a series of pulses of 0.12 cm^3 of a mixture of 5% vol CO/N_2 was injected successively into the reactor. The gaseous effluent from the reactor was passed through a methanator, where the non-adsorbed carbon monoxide was converted to methane, which was analyzed by gas chromatography using a FID. By counting the number of absorbed pulses, the total moles of adsorbed carbon monoxide were obtained. The metal dispersion was calculated by considering that carbon monoxide adsorption occurs in linear form on each exposed platinum atom.

The XPS spectra were acquired in a VG Scientific spectrometer Escalab model 220i-XL with source of X-ray, MgKα (1253 eV) anode and 4000 W power and hemispheric electron analyzer. The Al2p peak (BE = 74.5 eV) was chosen as an internal reference. This reference was in all cases in good agreement with the BE of the C1s peak arising from contamination, at 284.6 eV. This reference gives an accuracy of ±0.1 eV.

The activity of the metal sites was evaluated by dehydrogenation of cyclohexane to benzene, which is an insensitive reaction to the structure of the metal active site and thus the activity is known to be proportional to the number of surface active sites. The reaction was performed under the following conditions: catalyst weight = 0.1 g, 300 °C, 1 atm, H_2/CH (molar) = 3.4 and WHSV = 12.6. The catalyst was charged into a tubular fixed bed reactor and was reduced in situ under hydrogen flow (60 mL min^{-1}) for 2 h, at 600 °C, before each run. The products were analyzed in a Shimadzu GC-8A chromatograph equipped with a FID and a packed column of FFAP on Chromosorb. From the gas chromatography compositional data, the total conversion and the yield to benzene as reaction product were calculated on a carbon basis.

2.3. Catalytic evaluation

The catalysts were evaluated in methane steam reforming using a stainless steel microreactor and samples (0.15 g) previously reduced in situ under hydrogen flow at 600 °C, during 2 h. The reaction was carried out at 600 °C and 1 atm, using a steam to methane molar ratio of 4. A mixture of 10% methane in nitrogen was fed to a saturator (kept at 80 °C) and then to the reactor. Each run took 6 h and the products (hydrogen, carbon monoxide and carbon dioxide) as well as no reacted methane were analyzed in a Thermo Fennigan model Trace GC chromatograph, equipped with thermal conductivity detector (TCD), flame ionization detector FID) and methanator. The methane conversion was determined using Eq. (7), where X_{CH4} is the methane conversion and $n_{CH4(in)}$ and $n_{CH4(out)}$ are the inlet and outlet methane moles numbers, respectively. The selectivities to hydrogen (S_{H2}), carbon monoxide (S_{CO}) and to carbon dioxide (S_{CO2}) were calculated considering the balance of carbon atoms, according to Eqs. (8)–(10), respectively, where n_{CO} and n_{CO2} are the moles number of carbon monoxide and carbon dioxide, respectively.

$$X_{CH4}(\%) = (n_{CH4(in)} - n_{CH4(out)}) * 100/n_{CH4(in)} \quad (7)$$

$$S_{H2}(\%) = n_{H2(out)} * 100/2(n_{CH4(in)} - n_{CH4(out)}) \quad (8)$$

$$S_{CO}(\%) = n_{CO(out)} * 100/(n_{CH4(in)} - n_{CH4(out)}) \quad (9)$$

$$S_{CO2}(\%) = n_{CO2(out)} * 100/(n_{CH4(in)} - n_{CH4(out)}) \quad (10)$$

The hydrogen (Y_{H2}), carbon monoxide (Y_{CO}) and carbon dioxide (Y_{CO2}) yields were calculated considering the balance of carbon atoms, according to Eqs. (11)–(13), respectively.

$$Y_{H2}(\%) = n_{H2(out)} * 100/2n_{CH4(in)} \quad (11)$$

$$Y_{CO}(\%) = n_{CO(out)} * 100/n_{CH4(in)} \quad (12)$$

$$Y_{CO2}(\%) = n_{CO2(out)} * 100/n_{CH4(in)} \quad (13)$$

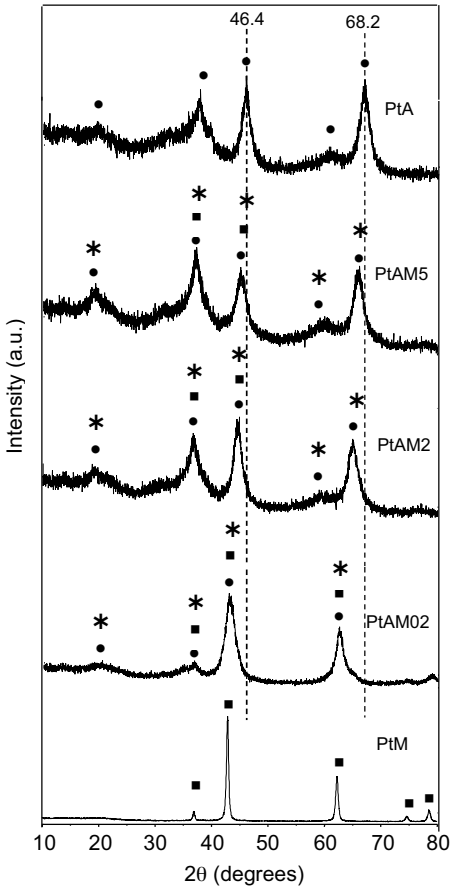

Fig. 1. X-ray diffractograms for PtA sample (alumina-supported platinum), PtM sample (magnesia-supported platinum) and for PtAM5, PtAM2 and PtAM02 samples: aluminum and magnesium oxide-supported platinum. The numbers indicate the aluminum to magnesium molar ratios. • γ-Al_2O_3; ■periclase (MgO); * $MgAl_2O_4$.

The coke amount on spent catalysts was measured in a LECO 200 model CS200 equipment, using a ceramic crucible containing 0.002 g of sample, 1.25 g a tungsten compound (Lecocel) and 1.25 g of accelerator to aid the combustion.

3. Results and discussion

The X-ray diffractograms of the catalysts are shown in Fig. 1. One can see that all spectra of alumina-containing catalysts showed broad peaks, indicating that poorly crystallized solids and/or with small crystallites were produced. On the other hand, the aluminum-free sample (PtM) showed a profile of a crystalline solid, characteristic of the periclase phase of magnesia (JCPDS 45-0946). The sample with the lowest amount of magnesium (Al/Mg = 5) showed a profile similar to the magnesium-free sample (PtA), which is characteristic of poorly crystallized γ-alumina (JCPDS 10-0414). It can be noted that the peaks related to alumina or to periclase can also be assigned to magnesium aluminate, $MgAl_2O_4$ (JCPDS 10-01238), for all aluminum and magnesium-based samples, making the phases identification difficult. Moreover, the peak at 68.2° for the PtA sample was shifted to lower angles for the aluminum and magnesium-based solids. This indicates the entrance of magnesium into alumina lattice, causing an increase of the interplanar distances. For the PtAM02 sample, this peak occurred at 61.8°, which is the value for periclase. Likewise, by adding alumina to magnesia-based catalyst (PtM), the peak at 62.7° of periclase was shifted to higher angles, indicating the entrance of aluminum in magnesia lattice. The presence of aluminum in magnesia lattice led

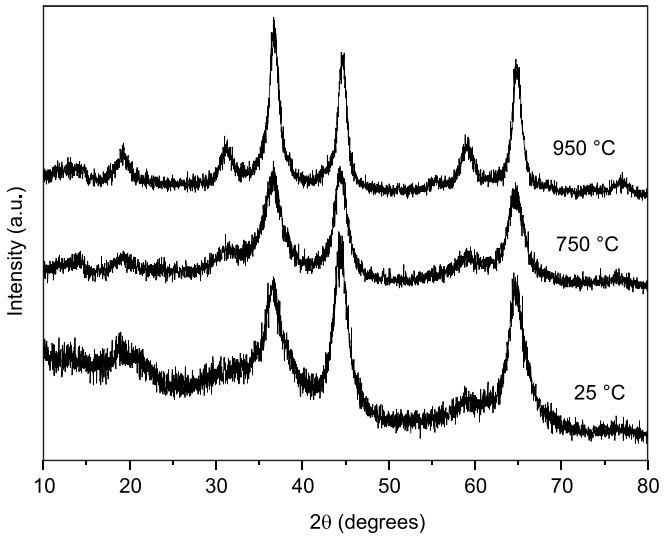

Fig. 2. X-ray diffractograms for the AM2 sample (Al/Mg = 2) taken at several temperatures.

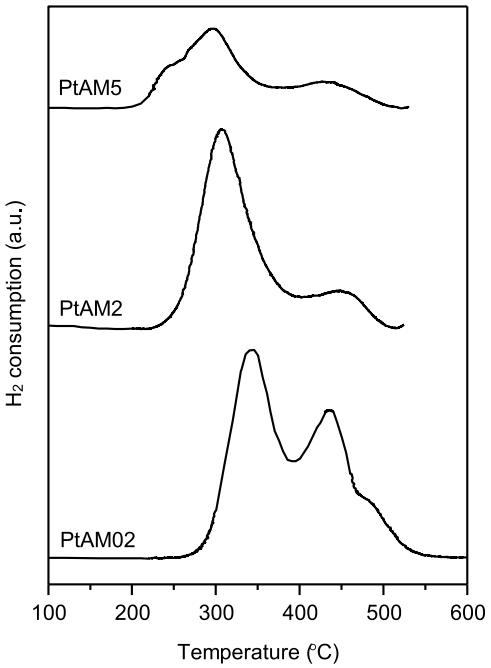

Fig. 3. TPR profiles for aluminum and magnesium oxide-supported platinum: PtAM02, PtAM02 and PtAM5 samples, with aluminum to magnesium molar ratios of 0.2, 2 and 5, respectively.

to a decrease in the lattice constant of magnesia, as found previously [25]. A similar behavior was noted for the peak at 46.4º. Therefore, one can conclude that the PtAM5 sample is mainly made of magnesium-containing alumina while the PtAM02 sample is made of aluminum-containing magnesia. The PtAM2 sample showed a profile that could be assigned to alumina, magnesia or magnesium aluminate. The production of magnesium aluminate at temperatures as low as 400 and 500 °C was also reported by other authors [26,27].

Fig. 2 showed the X-ray diffractograms collected at different temperatures after heating a selected sample (AM2) in situ. As we can see, the curves did not change upon heating, indicating that this solid was stable. Also, no change in the peaks broadening was found, showing that the crystallite size did not increase upon heating. These profiles are similar to those obtained by Guo et al. [28] and Grabowska et al. [27] heating the solids at 900 and 1100 °C, respectively and identifying the production of magnesium aluminate. These results suggest that our samples contain magnesium aluminate.

Table 1 shows the specific surface area of the supports and of the catalysts. The platinum impregnation caused a decrease in the specific surface area for the support with the highest Al/Mg molar ratio (AM5) and an increase for the support with the lowest molar ratio (AM02). For the solid with the intermediate Al/Mg molar ratio, the specific surface area did not change. The decrease in specific surface area can be related to the changes in the solids during impregnation, since the smallest particles of magnesia are expected to be dissolved by the acid solution of the chlorine-based precursor (H_2PtCl_6). During the reprecipitation process, particles with bigger size can be formed, decreasing the specific surface area of the solid. A similar effect was observed by other authors [29], during the impregnation of mixed oxides Mg(Al)O with palladium (II) chloride ($PdCl_2$). On the other hand, a considerable increase of the specific surface area for the PtAM02 sample was observed, as we can see in Table 1. This can be related to the higher ability of magnesia for adsorbing chlorine, due its basicity, as compared to alumina [29]. As this sample has the largest amount of magnesia, as compared to the other solids, it is able to retain more chlorine, which is released as hydrochloric acid, during the drying and calcination steps following impregnation, generating pores and then an increase in specific surface area.

Table 1
Specific surface areas (Sg) for the supports (AM5, AM2 and AM02) and for the catalysts and total acidity and metal dispersion (D) for the catalysts. PtA sample: alumina-supported platinum; PtM sample: magnesia-supported platinum; PtAM5, PtAM2 and PtAM02 samples: aluminum and magnesium oxide-supported platinum. The numbers represent the Al/Mg molar ratios.

Samples	Sg ($m^2\ g^{-1}$)	Total acidity (mmol NH_3 ads g^{-1})	D (%)
AM5	318	–	–
AM2	174	–	–
AM02	93	–	–
PtAM5	264	159	53.1
PtAM2	191	39.8	42.4
PtAM02	180	–	35.6
PtA	–	48.5	62.0
PtM	–	20.9	7.9

The temperature programmed reduction curves for the aluminum and magnesium-supported platinum are shown in Fig. 3. For all cases, a broad peak centered at around 300 °C can be noted, which can be associated with the reduction of platinum species in different interactions with the support. In the case of alumina-supported platinum, this peak usually occurs at temperatures in the range of 200–270 °C, as noted in previous works [4,30]. Therefore, magnesium made platinum reduction more difficult, this effect increasing with its content. This indicates that magnesium increased platinum-support interaction. For the PtAM5 curve, a shoulder at 241 °C can be seen, which is associated to the reduction of surface oxychlorated platinum species [4]. Another peak at about 425 °C is related to the reduction of platinum crystals in strong interaction with the support [30,31], this peak increasing with magnesium amount.

The total hydrogen consumption in the reduction of PtAM5 sample corresponds to the stoichiometric value (102.5 μmol H_2 $gcat^{-1}$) for the total reduction of platinum going from the (IV) to the (0) oxidation state. On the other hand, in the case of the samples with the highest magnesium contents (PtAM2 and PtAM02), the total hydrogen consumption (120 μmol H_2 $gcat^{-1}$ and 127 μmol H_2 $gcat^{-1}$, respectively) overcame the stoichiometric value for reducing all platinum species. Since pure alumina and magnesia cannot be reduced in the experimental conditions, the extra hydrogen

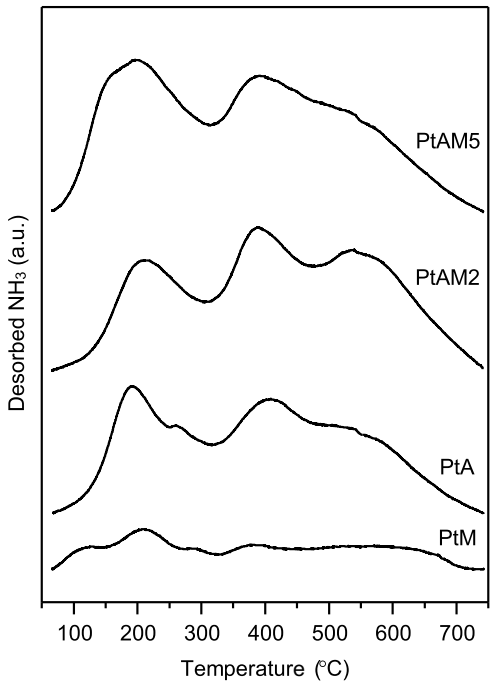

Fig. 4. TPD/NH_3 profiles for alumina-supported platinum (PtA), magnesia-supported platinum (PtM) and alumina and magnesia-supported platinum (PtAM02, PtAM2 and PtAM5). The numbers indicate the aluminum to magnesium molar ratio.

consumption can be attributed to the reduction of small amounts of impurities on the support, which was catalyzed by platinum, as found previously [12].

The TPD-NH_3 curves of the catalysts are shown in Fig. 4 and the values of total acidity are displayed in Table 1. Taking the PtA catalyst as a reference, we note that the first peak was shifted to higher temperatures and the second one to lower temperatures for the magnesium-containing samples. Since the desorption temperature is related to the strength of the acid sites [32,33], it means that magnesium affects the distribution of the acid sites, increasing the strength of the weak sites and decreasing the strength of the strong and moderate sites.

From Table 1, one can note that the total acidity of the PtA catalyst changed by magnesium addition depending on its amount. Small amounts of magnesium (Al/Mg = 5) cause an increase of the total amount of acid sites. However, higher amounts of magnesium (Al/Mg = 2) decreased the total acidity. These results are in accordance with previous works [32,33], which claimed that the acid properties of MgO-Al_2O_3 can be tailored by using appropriate amounts of magnesia and alumina. Therefore, the addition of small amounts of magnesium (basic) to alumina (amphoteric) increased the total acidity, generating weak and moderate acidity by neutralizing some alumina strong sites. This explains the increase in the total acidity of the PtAM5 catalyst as compared to the PtA sample. On the other hand, the magnesium content was higher for the PtAM2 catalyst and then the magnesium oxide basic strength contributed more for decreasing the total acidity of this solid. Pure magnesia does not have inherent acidity but the addition of platinum created acid sites on the solid surface due to the acid nature of platinum oxychloride species, which can remain in the solid. This explains the acidity found for the PtM sample. A similar effect was observed in a previous work [34], by adding 8% of molybdenum to magnesia, which increased the total acidity and changed the distribution of acid sites.

The FTIR spectra of the chemisorbed carbon monoxide on platinum surface (Fig. 5) showed a broad band in the range from 2150 to 1980 cm^{-1}. For the PtA sample, the

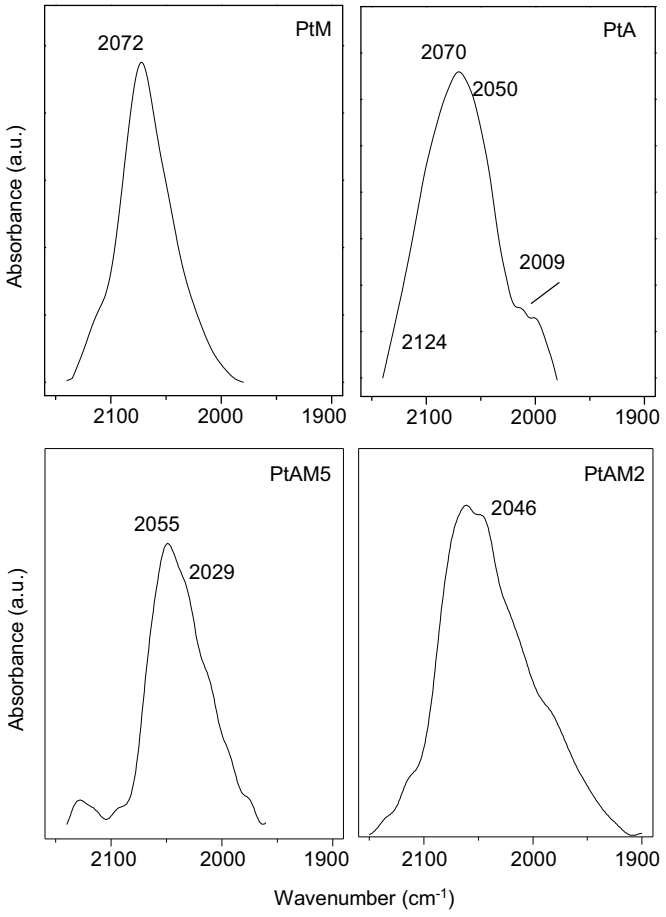

Fig. 5. FTIR of carbon monoxide adsorbed on alumina-supported platinum (PtA), magnesia-supported platinum (PtM) and alumina and magnesia-supported platinum (PtAM2 and PtAM5). The numbers indicate the aluminum to magnesium molar ratio.

deconvolution of the bands produced components at 2124, 2070, 2050, and 2009 cm^{-1}, which are associated to carbon monoxide linearly bonded on metallic platinum in different electronic states [35]. For all magnesium-containing catalysts, these bands were shifted to lower wavenumbers, indicating an electronic enrichment of the superficial platinum atoms due to the addition of magnesium. This finding can be associated to the higher ability of magnesia for adsorbing chlorine as compared to alumina [29], suggesting that the hexachloroplatinate ions ($PtCl_6]^{2-}$) were adsorbed more on divalent magnesium than on trivalent aluminum ions, leading to the production of more platinum richer in electrons.

Fig. 6 shows the conversion of cyclohexane to benzene as a function of time. Alumina-supported platinum catalyst led to the highest conversions while magnesia-supported platinum led to the lowest values. The magnesium-containing samples led to intermediate values. It can be noted that the conversion decreased with increasing magnesium content in the solids. These results are in accordance to the dispersion measurements, as shown in Table 1. As pointed out early [31], when platinum is electronically enriched ($Pt^{\delta-}$) it shows smaller hydrogen chemisorption and catalytic activity as compared to Pt^0. Therefore, the electronic effect is stronger than the geometric effects during the model reaction of cyclohexane dehydrogenation. As found by FTIR, the addition of magnesium to alumina-supported platinum caused an electronic enrichment of platinum and then a decrease in the dehydrogenation activity and in the hydrogen chemisorption.

The binding energies (BE) of some characteristic core levels of Mg, Al, Pt and O for the samples are displayed in Table 2. The

Table 2
Binding energies and surface atomic ratios for the catalysts. PtA sample: alumina-supported platinum; PtM sample: magnesia-supported platinum; PtAM5, PtAM2 and PtAM02 samples: aluminum and magnesium oxide-supported platinum. The numbers represent the Al/Mg molar ratios.

Samples	Binding energies (eV)				Surface atomic ratios			
	Mg2p	Al2p	Pt4d	O1s	Al/Mg	Pt/Al	Pt/Mg	Pt/(Al + Mg)
PtA	–	74.3	316.0	533.6	–	0.000118	–	0.000118
PtAM5	50.2	74.5	316.0	531.7	1.730	0.00543	0.009417	0.00344
PtAM2	50.6	73.7	316.0	532.3	1.801	0.00183	0.003307	0.00118
PtAM02	51.3	74.5	316.0	532.9	0.408	0.000345	0.000141	0.000100
PtM	51.8	–	316.0	531.5	–	–	0.000275	0.000275

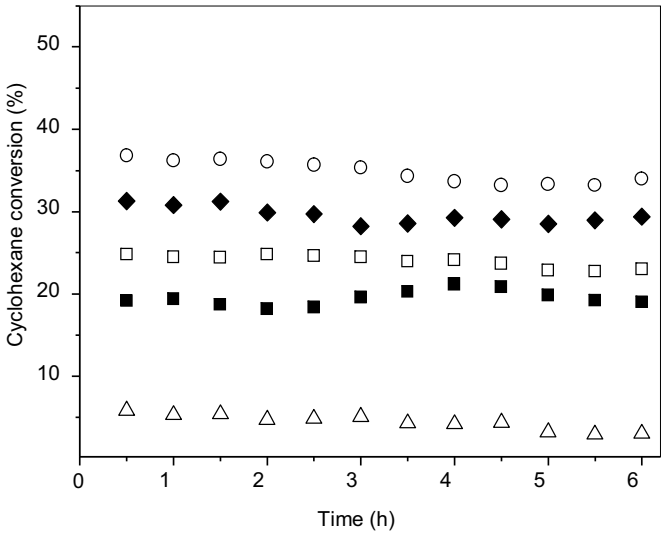

Fig. 6. Cyclohexane conversion as a function of time on (○) alumina-supported platinum (PtA sample), (△) magnesia-supported platinum (PtM) and on alumina and magnesia-supported platinum with (■) Al/Mg = 0.2 (PtAM02); (□) Al/Mg = 2.0 (PtAM2) and (♦) Al/Mg = 5.0 (PtAM5).

binding energies for the Al 2p peaks were in close agreement with that for Al^{3+} in Al_2O_3 or $MgAl_2O_4$ type compounds [36–38]. In addition, the Mg2p binding energy for PtM sample is typical of Mg^{2+} species in magnesia [38]. It can be noted that these values decreased with increasing aluminum content, indicating the production of $MgAl_2O_4$ spinel [37]. The Mg2p binding energy for the PtAM2 sample is quite close to the value for magnesium aluminate (50.5 eV) [36]. These findings are in agreement with the X-ray diffraction results.

The binding energy for the O1s peak in magnesia supported-platinum was typical of oxygen in magnesia [39]. In addition, the value is characteristic of oxygen in alumina for the alumina-supported platinum [40]. For the aluminum and magnesium-containing catalysts, the binding energies for the Os1s peak changed with the sample composition indicating that the chemical state of the oxygen species on the surface depends on the chemical composition of the solids. The values increased with aluminum concentration, as found in previous works [26,41]. This can be related to the entrance of aluminum in magnesia lattice in accordance with the X-ray results. The values of binding energy Pt4d for all samples are typical of Pt^{4+} species in platinum oxide (PtO_2) [38].

Table 2 also shows the chemical composition on the surface for the catalysts. It can be noted that the PtAM2 sample (Al/Mg = 2) showed the aluminum-richest surface, followed by the PtAM5 and PtAM02 samples. One can also observe that the PtAM02 sample has higher Al/Mg ratio on the surface (0.408) than expected in the bulk (0.20) indicating an inhomogeneous distribution of aluminum in solids with accumulation on the surface. The tendency of aluminum to go to the surface in aluminum and magnesium-based solids was also observed by other authors [26]. An opposite behavior was noted for the PtAM5 sample, for which the amount of aluminum on the surface (Al/Mg = 1.730) was lower than that expected in the bulk (Al-Mg = 5). In this case, the amount of aluminum is close to magnesium aluminate, suggesting the production of magnesium aluminate on the surface. On the other hand, the PtAM2 sample showed around the same amount of aluminum and magnesium on the surface (1.801) and in the bulk (Al/Mg = 2), indicating a homogenous distribution of the metals in the solids. This amount is close to the value of magnesium aluminate, suggesting that this solid is made of the spinel, in accordance with the X-ray diffraction and XPS results. Therefore, one can suppose that the surface of PtAM2 and PtAM5 samples is made of magnesium aluminate whereas the surface of PtAM02 sample is made of magnesium aluminate and magnesia. This result is in accordance with the lowest acidity of the sample as compared to the other aluminum and magnesium-based solids. The highest amount of platinum on the surface was found for the PtAM5 sample and decreased with the increase of magnesium in solids, in agreement with the values of metal dispersion (Table 1) and of the cyclohexane conversions (Fig. 6). These results can be assigned to the specific surface areas of the supports (Table 1) for which the same tendency was noted.

Fig. 7 shows the methane conversion, hydrogen selectivity, carbon monoxide selectivity, carbon dioxide selectivity and hydrogen to carbon monoxide molar ratio over the catalysts as a function of reaction time. The catalyst with the lowest amount of magnesium (PtAM5 sample) led to the highest initial conversion, a fact that can be related to the highest amount of platinum on the surface (Table 2) as well as to the high reducibility of platinum, as found by TPR. Alumina-supported platinum (PtA) and magnesia-supported platinum (PtM) led to close initial conversions but have different amounts of platinum on the surface, the magnesia-supported platinum showing the highest amount. This finding can be explained by considering that the electronic state of platinum changed due to magnesium. As found by TPR, platinum becomes electronically enriched ($Pt^{\delta-}$) due to magnesium and then its hydrogen chemisorption and catalytic activity is decreased, as found by dispersion measurements and cyclohexane dehydrogenation, respectively. This means that platinum atoms on magnesia surface are less active than on alumina. Therefore, more atoms on magnesia surface are needed to produce methane conversions similar to alumina-supported platinum. In addition, the support is believed to play a role on the catalytic activity especially in water chemisorption, in accordance with previous works [12,42]. It is generally accepted [43,44] that the steam reforming reaction takes place at the metal-support interface, by the reaction between methane (preferentially adsorbed on the metal) and water (preferentially adsorbed on the support), which dissociates and generates oxygen species. Also, it is well-known [42] that alkaline earth oxides, such as magnesium oxide, calcium oxide and barium oxide are often incorporated into steam reforming catalysts to provide operational advantages resulting from lower support acidity, higher metal dispersions and improved steam activation. In addition, it was pointed out [31] that basic supports tend to donate electron to the metal, decreasing the activity, in agreement with

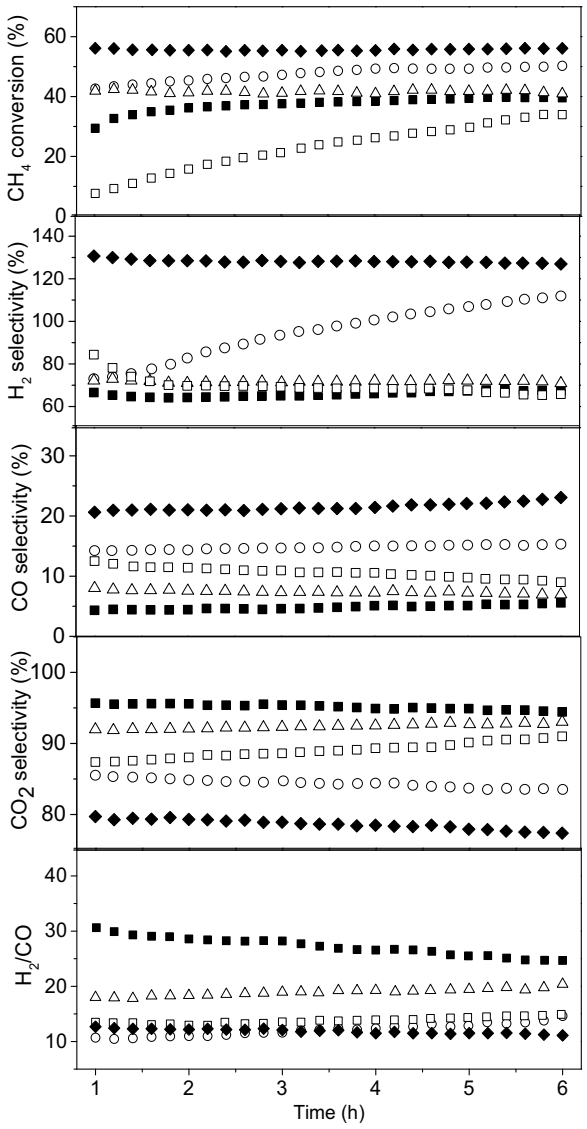

Fig. 7. Methane conversion, hydrogen selectivity, carbon monoxide selectivity, carbon dioxide selectivity and hydrogen to carbon monoxide molar ratio as a function of time during methane steam reforming on (○) alumina-supported platinum (PtA sample), (△) magnesia-supported platinum (PtM) and on alumina and magnesia-supported platinum with (■) Al/Mg = 0.2 (PtAM02); (□) Al/Mg = 2.0 (PtAM2) and (♦) Al/Mg = 5.0 (PtAM5).

our results of cyclohexane dehydrogenation. This explains why the PtM sample has more platinum on the surface but has the same activity as the PtA sample. The PtAM02 and PtAM2 samples were the least active catalysts. These solids have quite different surfaces, the first one showing magnesium aluminate, magnesia and more platinum than the other one, which has only magnesium aluminate, besides platinum. For these catalysts, magnesium was also acting as electron donator for platinum and then the activity decreased.

From Fig. 7, we can also see that the conversion changed with reaction time, depending on the catalyst. The sample with the lowest amount of magnesium (PtAM5) was stable during reaction while the activity of the magnesia-supported platinum slightly decreased with time. On the other hand, the activity of the other catalysts increased during reaction, indicating an increase of active sites by the slow reduction of platinum by hydrogen came from methane decomposition, as found previously for nickel-based catalyst [9]. After 6 h on stream, the magnesium-richest samples (PtM and PtAM02) led to similar values of conversions.

Table 3
Methane conversion (X), selectivity to hydrogen (S_{H2}), carbon monoxide (S_{CO}) and carbon dioxide (S_{CO2}), hydrogen to carbon monoxide molar ratio and amount of carbon (C) on the spent catalysts after 6 h on stream. PtA sample: alumina-supported platinum; PtM sample: magnesia-supported platinum; PtAM5, PtAM2 and PtAM02 samples: aluminum and magnesium oxide-supported platinum. The numbers represent the molar ratios of Al/Mg.

Catalyst	X (%)	S_{H2} (%)	S_{CO} (%)	S_{CO2} (%)	H_2/CO	C (%)
PtA	50	100	15	85	15	0.27
PtAM5	56	100	23	77	11	0.08
PtAM2	34	66	9	91	15	0.42
PtAM02	40	67	5.6	94	24	0.60
PtM	41	71	7	93	20	0.10

The values of selectivity to hydrogen followed a similar tendency, as shown in Fig. 7. The catalyst with the lowest amount of magnesium (PtAM5 sample) was the most selective to hydrogen followed by alumina-supported platinum (PtA). However, the magnesium-richest catalysts (PtM, PtAM02 and PtAM2) showed similar values at the end of reaction.

Fig. 7 also shows the selectivities of the catalysts to carbon monoxide and carbon dioxide as a function of reaction time. As we can see, all catalysts showed low selectivities to carbon monoxide and high selectivities to carbon dioxide, indicating the occurrence of the water gas shift reaction (Eq. (2)) under the operation conditions. The activity of platinum in the WGSR was previously demonstrated [45]. The PtAM02 sample showed the highest selectivities to carbon dioxide and the lowest selectivities to carbon monoxide, indicating that it was the most active in WGSR. On the other hand, PtAM5 sample showed an opposite behavior and was the least active in WGSR. It can be noted that the increasing of magnesium amount increased the activity of the catalysts in WGSR. As magnesium is expected to decrease the activity because of the electronic enrichment of platinum, this finding can be related to the role of the support in the water adsorption during the WGSR.

The differences in activity of the catalyst in WGSR allow the tailoring of the catalyst to obtain different hydrogen to carbon monoxide molar ratio for several purposes. As shown in Fig. 7, the addition of small amount of magnesium to alumina-based sample (PtA) generating the Pt/AM5 sample, leads to a slight decrease of H_2/CO ratio. However, the addition of higher amount (Pt/AM2) leads to slight increase while even higher amounts lead to almost a doubled increase. As a consequence of the highest activity of the Pt/AM02 sample in WGSR, it produced the highest value of H_2/CO ratio.

Table 3 shows the values of methane conversions over the catalysts and the selectivities towards the products after 6 h on stream. The PtAM5 and PtA samples led to the highest methane conversions, which was around five times the conversion obtained over a commercial catalyst based on nickel evaluated under in the same reaction conditions (10%). The solids with the lowest Al/Mg molar ratios led to similar conversions to the magnesia-supported platinum, which in turn was less active and selective to hydrogen than the PtA sample. All catalysts were more selective to carbon dioxide than to carbon monoxide, indicating that they more active in the WGSR than in methane reforming. The values of hydrogen to carbon monoxide molar ratio, obtained in the outlet of the reactor after 6 h on stream, showed that the aluminum-richest samples (PtA, PtAM5 and PtAM2) samples led to the lowest values. On the other hand, the other samples led to higher values, indicating that they were more active in WGSR than the other samples. Table 3 also shows the carbon content on the spent catalysts, after 6 h of methane steam reforming reaction. It can be noted that very small amounts of coke were produced on the catalysts, probably because the acid sites of the catalysts were mostly weak or moderate. This finding indicates

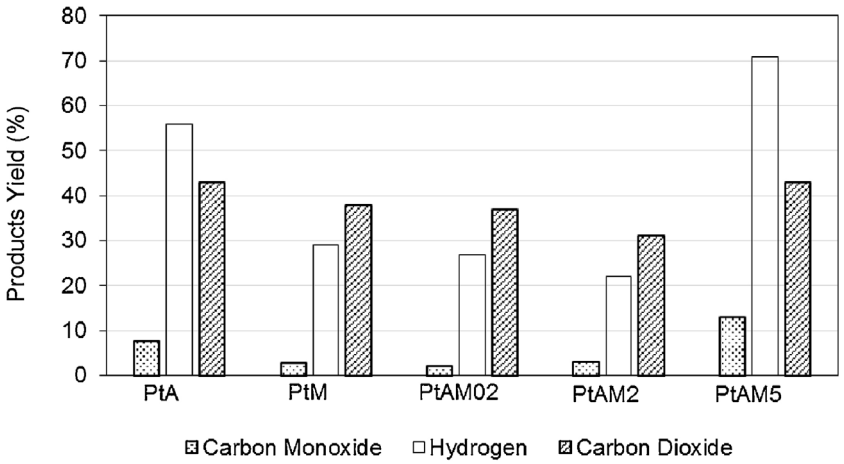

Fig. 8. Hydrogen, carbon monoxide and carbon dioxide yields after 6 h on stream during methane steam reforming on alumina-supported platinum (PtA sample), magnesia-supported platinum (PtM) and alumina and magnesia-supported platinum with Al/Mg = 0.2 (PtAM02); Al/Mg = 2 (PtAM2) and Al/Mg = 5 (PtAM5).

the benefic combination of magnesium and platinum to prevent coke formation.

Fig. 8 shows the products yield obtained over the catalysts. One can see that the aluminum-richest samples (Pt/AM5 and Pt/A) led to the highest hydrogen yields. These samples produce similar hydrogen to carbon monoxide ratios but the magnesium-containing sample led to the highest hydrogen yield being the best candidate for hydrogen production.

4. Conclusions

Magnesium affects the properties of Pt/-Al_2O_3 catalyst depending on the amount. In small contents (Al/Mg (molar) = 5), magnesium enters into alumina lattice and produces magnesium aluminate on the surface while in higher amounts (Al/Mg (molar) = 2) a solid made of magnesium aluminate is obtained. In even higher contents (Al/Mg (molar) = 0.2) aluminum enters into magnesia lattice and produces a solid with magnesia and magnesium aluminate on the surface. Magnesium changed the specific surface area and the acidity of the solids depending on the composition, the aluminum-richest catalyst (Al/Mg = 5) showing the highest values. Platinum dispersion follows the same tendency. In addition, magnesium causes an electronic enrichment of platinum and increases the interaction of platinum with the support making the reduction more difficult. These changes affect the activity and selectivity of the catalysts in methane steam reforming and in water gas shift reaction, leading to different products yield and different hydrogen to carbon monoxide molar ratios. Therefore, the catalysts can be tailored for different purposes. Among the obtained catalysts, the sample with Al/Mg = 5 is the best option to obtain hydrogen.

Acknowledgments

ARM and LSC are grateful to CNPq and to FAPESB for the scholarships. The authors thank to FINEP, CNPq and FAPESB for the financial support and to Instituto Venezolano de Investigaciones Científicas (Venezuela) for XPS analyses.

References

[1] B. Viswanathan, Energy Sources (2017) 161–183.
[2] C. Gómez-Solís, S.L. Peralta-Arriaga, L.M. Torres-Martínez, I. Juárez-Ramírez, L.A. Díaz-Torres, Fuel 188 (2017) 197–204.
[3] B. Viswanathan, Energy Sources (2017) 185–212.
[4] M.C. Rangel, L.S. Carvalho, P. Reyes, J.M. Parera, N.S.F. Ígoli, Catal. Lett. 64 (2000) 171–178.
[5] E. Moniz, A. Meggs, G.S. MCrae, C. Ruppel, The Future of Natural Gas, An Interdisciplinary MIT Study, Cambridge, 2011.
[6] J.R. Rostrup Nielsen, J. Schested, Adv. Catal. 47 (2002) (165-139).
[7] D.L. Trimm, Catal. Today 49 (1999) 3–10.
[8] L.N. Bobrova, V.A. Sadykov, N.V. Mezentseva, V.V. Pelipenko, N.V. Vernikovskaya, O.P. Klenov, O.L. Smorygo, Int. J. Hydrogen Energy 41 (2016) 4632–4645.
[9] S.P. de Lima, V. Vicentini, J.L.G. Fierro, M.C. Rangel, Catal. Today 133–135 (2008) 925–930.
[10] J.S. Moura, M.C. Rangel, M.O.G. Souza, Fuel 87 (2008) 3627–3630.
[11] L.C.P. Fernandes Junior, S. de Miguel, J.L.G. Fierro, M.C. Rangel, Stud. Surf. Sci. Catal. 167 (2007) 499–504.
[12] L.S. Carvalho, A.R. Martins, P. Reyes, M. Oportus, A. Albonoz, V. Vicentini, M.C. Rangel, Catal. Today 142 (2009) 52–60.
[13] Y. Khani, Z. Shariatinia, F. Bahadoran, Chem. Eng. J. 299 (2016) 353–366.
[14] M. Németh, Z. Schay, D. Srankó, J. Károlyi, G. Sáfrán, I. Sajó, A. Horváth, Appl. Catal. A: Gen. 504 (2015) 608–620.
[15] J. Niu, X. Du, J. Ran, R. Wang, Appl. Surf. Sci. 376 (2016) 79–90.
[16] M. Geske, K. Peelzer, R. Horn, F.C. Jentoft, R. Schlögl, Catal. Today 42 (2009) 61–69.
[17] A. Bitsch-Larsen, R. Horn, L.D. Schmidt, Appl. Catal. A: Gen. 348 (2008) 165–172.
[18] Y. Mukainakano, K. Yoshida, S. Kado, K. Okumura, K. Kunimori, K. Tomishige, Chem. Eng. Sci. 63 (2008) 4891–4901.
[19] G. Jacobs, R.A. Keogh, B.H. Davis, J. Catal. 245 (2007) 326–337.
[20] P. Tolmacsov, A. Gazsi, F. Solymosi, Appl. Catal. A: Gen. 362 (2009) 58–61.
[21] A. Seretis, P. Tsiakaras, Renew. Energy 85 (2016) 1116–1126.
[22] G. Guan, M. Kaewpanha, X. Hao, A. Abudula, Renew. Sustain. Energy Rev. 58 (2016) 450–461.
[23] M.A. Aramendía, J.A. Benítez, V. Borau, C. Jiménez, J.M. Marinas, J.M. Porras, J.R. Ruiz, F.J. Urbanos, Colloids Surf. A: Physicochem. Eng. Aspects 225 (2003) 137–143.
[24] A.D. Mazzoni, M.A. Sainz, A. Caballero, E.F. Aglietti, Mater. Chem. Phys. 78 (2003) 30–37.
[25] T. Sato, H. Fujita, T. Endo, M. Shimada, React. Solids 5 (1988) 219–228.
[26] D. Cosimo, V. Díez, E. Iglesias, C. Apesteguía, J. Catal. 178 (1998) 499–510.
[27] H. Grabowska, M. Zawadzki, L. Syper, W. Mišta, Appl. Catal. A: Gen. 292 (2005) 208–214.
[28] J. Guo, H. Lou, H. Zhao, D. Chai, X. Zheng, Appl. Catal. A: Gen. 273 (2004) 75–82.
[29] F. Prinetto, M. Manzoli, G. Ghiotti, J.M. Ortiz, D. Tichit, B. Coq, J. Catal. 222 (2004) 238–249.
[30] L.S. Carvalho, P. Reyes, G. Pecchi, N.S. Figoli, C.L. Pieck, M.C. Rangel, Ind. Eng. Chem. Res. 40 (2001) 5557–5563.
[31] L.S. Carvalho, C.L. Pieck, M.C. Rangel, N.S. Figoli, J.M. Grau, P. Reyes, J.M. Parera, Appl. Catal. A: Gen. 269 (2004) 91–103.
[32] J.S. Moura, M.O.G. Souza, J.D.A. Bellido, E.M. Assaf, M. Opportus, P. Reyes, M.C. Rangel, Int. J. Hydrogen Energy 37 (2012) 3213–3224.
[33] M. Kumar, F. Aberuagba, J.K. Grupta, K.S. Rawat, L.D. Sharma, G.M. Dhar, J. Mol. Catal. A: Chem. 213 (2004) 217–223.
[34] K.V.R. Chary, H. Ramakrishna, K.S.R. Rao, G.M. Char, G.P.K. Rao, Catal. Lett. 10 (1991) 27–34.
[35] M.C.S. Santos, J.M. Grau, C.L. Pieck, J.M. Parera, J.L.G. Fierro, N.S. Fígoli, M.C. Rangel, Catal. Lett. 103 (2005) 229–237.
[36] C.D. Wagner, W.M. Riggs, L.E. Davis, J.F. Moulder, G.E. Muilenberg, Handbook of X-Ray Photoelectron Spectroscopy, Perkin-Elmer Coorporation, Eden Prairie, 1978.
[37] K.Z. Chong, T.S. Shih, Mater. Chem. Phys. 80 (2003) 191–200.
[38] G. Corro, J.L.G. Fierro, V.C. Odilon, Catal. Commun. 4 (2003) 371–376.

[39] C.D. Wagner, L.E. Davis, M.V. Zeller, J.A. Taylor, R.H. Raymond, L. Gale, Surf. Interface Anal. 3 (1981) 211–225.
[40] F.J. Sebastián, C. Maffiotte, J.C. Galván, A. Pardo, M.C. Merino, R. Arraba, Open Surf. Sci. J. 3 (2011) 1–14.
[41] G.D. Cantrell, L.J. Gillie, A.F. Lee, K. Wilson, Appl. Catal. A: Gen. 287 (2005) 183–190.
[42] J.T. Richardson, B. Turk, M.W. Twigg, Appl. Catal. A: Gen. 148 (1996) 97–112.
[43] J.R. Rostrup Nielsen, J. Sehested, J.K. Nørskov, Adv. Catal. 47 (2002) 65–139.
[44] F. Melo, N. Morlanés, Catal. Today 133–135 (2008) 383–393.
[45] P.S. Querino, J.R.C. Bispo, M.C. Rangel, Catal. Today 108 (2005) 920–925.